

Free vibration and wave power reflection in Mindlin rectangular plates via exact wave propagation approach

Seyyedmostafa Mousavi Janbehsarayi ¹, Arian Bahrami ^{*,2}, Mansour Nikkhah Bahrami¹

¹Department of Mechanical Engineering, College of Engineering, University of Tehran, Tehran, Iran.

²Department of Mechanical Engineering, Eastern Mediterranean University, G. Magosa, TRNC Mersin 10, Turkey. E-mail: arian.bahrami@emu.edu.tr

Abstract

Reflection, propagation and energy analysis are crucially important in designing structures, especially plates. A thick plate is considered based on first order shear deformation theory. Wave Propagation Method (WPM) is employed to exactly derive resonant frequencies and wave power reflection from different classical boundary conditions. Firstly, the frequency results are compared with other literatures to validate the exact proposed wave solution in the present work. Then, wave analysis and benchmark results for natural frequencies are presented for six different combinations of boundary conditions. The results indicate that the wave power reflection of thick rectangular plates is quite complicated and an incident wave of a specific type gives rise to other types of waves except for simply supported boundary conditions where the reflected wave power does not depend on the system parameters.

Keywords: Wave propagation method, Wave motion, Power reflection, Frequency analysis

1. Introduction

Rectangular plates have extensive application in engineering from Nanotechnology [1] to Aerospace [2] and Biomechanics [3] and many others. Their responses to an external excitation and energy transmission to their neighborhoods must be studied carefully to avoid any probable damage [4].

Many researches have contributed to study the vibration of thin plates such as Leissa's exact solution [5]. Yet, the dynamics of thick plates is quite complex due to the variation of shear deformation across the thickness and effect of inertia forces [6]. Precedent studies in this field done by Reissner [7] and Mindlin [8]. Mindline plate theory, also known as first-order shear deformation theory (FSDT), considers the distribution of shear deformation across the thickness as a linear function and solves the obtained three equations of the motion. Total deflection of the plate consists of bending deflection, shear contribution and angles of rotation. Based on which of the mentioned parameters are considered as fundamental variables, the strategy for deriving the equation(s) of the motion will be determined, considering the fact that reducing the fundamental variables, and consequently equations of the motion will simplify the solution [9,10]. Although numerous analytical and numerical methods have been presented, most of them have limited applications [11,12]. Higher order shear deformation theories (HSDT) involve higher-order expansion of the displacements. This assumption increases the number of unknowns; Murty's theory of HSDT [13] deals with 5, 7, 9 unknowns, Kant [14] with 6 unknowns, and Lo et al. [15] with 11 unknowns.

Numerical and semi-analytical methods come in handy when the complexity of a problem precludes the analytical approaches to be used. The FEM and Rayleigh-Ritz energy methods are two major procedures for solving the obtained equations of the motion. The proposed solutions based on FEM method are able to solve the vibration of moderately thick plates with any

combinations of boundary conditions [16]. Yet, shear locking problem is one of their salient concerns due to coupling between bending and shear modes [17]. Recently, Senjanović et al. [18] proposed a shear-locking-free FEM method for vibration analysis of Mindlin plates using bending deflection as a potential function for the definition of total deflection and angles of cross-section rotations. The Rayleigh-Ritz energy method [19-21] and boundary characteristic orthogonal polynomials along with three-dimensional Ritz formulation [22,23] have been used for the free vibration analysis of thick plates with arbitrary boundary conditions. The accuracy of the results is sensitive to the assumed natural modes presented by set of orthogonal functions. Hashemi et al. [24] proposed an exact analytical Levy type solution for thick plates using FSDT. They investigated the free vibration of moderately thick rectangular plates for six combinations of boundary conditions. There are also several other methods for vibration analysis of Mindlin-Reissner plates such as cell-based smoothed radial point interpolation method [25], discrete singular convolution method [26].

In addition to the methods mentioned above, there exists an exact approach known as wave propagation method (WPM). WPM is a simple, non-iterative, and efficient method for obtaining the natural frequencies of a system. Instead of applying boundary conditions to equations of the motion, reflecting, transmitting and propagating waves will be investigated to determine the natural frequencies and mode shapes of a system. One of the advantages of this method is the ability to study the energy transmission to the neighbors. This is very important for designing structures, because the effect of vibration to the neighbors and bases at frequencies near the natural frequencies will be determined prior to the construction. Wave propagation approach has been utilized mainly for finding the natural frequencies of beams, thin plates, rectangular and circular shells, membranes, frames, Nano-materials, and composite structures. Study of transmission and

reflection matrices in Euler-Bernoulli [27] and Timoshenko [28] beams are two cases of WPM method application in beam theories. Bahrami et al. [29] used modified wave approach to find the natural frequencies of non-uniform beams, using Euler-Bernoulli beam theory. In another work, Bahrami et al. [30] used WPM for free vibration of non-uniform rectangular membranes. Annular circular and sectorial membranes were studied in [31,32] using two dimensional wave propagation. Also, the nonlocal scale effect on buckling, vibration and wave reflection in beams has been studied in [33,34]. The authors showed that, in nanotubes, the reflected power of an incident wave, except for simply supported boundary condition, is dependent upon the small scale parameter and incident wave frequency. Moreover, Bahrami studied the free vibration, wave power transmission and reflection in multi-cracked nanobeams [35] and nanorods [36]. Furthermore, Bahrami and Teimourian [37] presented the small scale effect on vibration and wave power reflection in circular annular thin nanoplates. Recently, Ilkhani et al. [38] studied energy reflection and transmission in rectangular thin nanoplates. They showed that except for simply supported boundary condition, in other conditions, the obtained coefficients of the transmission matrix, and consequently the energy reflection is dependent on the non-dimensional frequency parameter of the incident wave, the non-dimensional nonlocal parameter, the thickness to length ratio and the number of half waves in length direction.

Reviewing the above acknowledged literature provides us the clue that there is no research conducted on wave analysis and investigation of the effect of thickness of the plate on wave motion, conversion and reflection in thick plates. In all previously done researches in wave analysis of structures, there were at most two waves [27-38] while here there are three waves, and this makes the problem more complicated to analyze. In the present paper, a new analytical approach to analyze the free vibration and wave reflection in thick rectangular plates is presented

using wave propagation method. In section 2, the governing equations of the motion with free, simply supported, and clamped boundary conditions are developed; the equations of the motion are rewritten in a specific format compatible with Wave Propagation Method (WPM). In this section, first, the equations of the motion are used to derive the exact propagation matrix, then exact reflection matrices are derived for mentioned boundary conditions. In addition, the propagation and reflection matrices will be helpful for future works that has to do with wave power transmission and reflection in waveguide structures. In section 3, numerical results are presented and investigated. The results are compared with other literatures and exact benchmark results are presented for the natural frequency for various aspect ratios, thickness to length ratios, and boundary conditions. As they are considered to be exact results, other researchers can use them to verify their approximate solutions in future works. Finally, the behavior of the reflection matrices is discussed for different boundary conditions. These results are discussed thoroughly for different thickness to length ratios and frequency ranges. Various boundary conditions are also considered to analyze the wave power reflection at boundaries. These results depict the behavior of the reflection coefficients which shows the energy reflected and dissipated at boundaries.

2. Methodology

2.1 Governing equation of motion

The non-dimensional equations of motion based on Mindlin plate theory for a flat, isotropic, thick rectangular plate of length a , width L and thickness h as shown in Fig.1 are [24]:

$$\tilde{\psi}_{1,11} + \eta^2 \tilde{\psi}_{1,22} + \frac{\nu_2}{\nu_1} (\tilde{\psi}_{1,11} + \eta \tilde{\psi}_{2,12}) - \frac{12K^2}{\delta^2} (\tilde{\psi}_1 - \tilde{\psi}_{3,1}) = -\frac{\beta^2 \delta^2}{12\nu_1} \tilde{\psi}_1, \quad (1a)$$

$$\tilde{\psi}_{2,11} + \eta^2 \tilde{\psi}_{2,22} + \frac{\nu_2}{\nu_1} \eta (\tilde{\psi}_{1,12} + \eta \tilde{\psi}_{2,22}) - \frac{12K^2}{\delta^2} (\tilde{\psi}_2 - \eta \tilde{\psi}_{3,2}) = -\frac{\beta^2 \delta^2}{12\nu_1} \tilde{\psi}_2, \quad (1b)$$

$$\tilde{\psi}_{3,11} + \eta^2 \tilde{\psi}_{3,22} - (\tilde{\psi}_{1,1} + \eta \tilde{\psi}_{2,2}) = -\frac{\beta^2 \delta^2}{12K^2 \nu_1} \tilde{\psi}_3 \quad (1c)$$

where $\delta = \frac{h}{a}$ is the dimensionless thickness to length ratio, $\eta = \frac{a}{b}$ is aspect ratio, $\beta = \omega a^2 \sqrt{\frac{\rho h}{D}}$ is the non-dimensional frequency parameter, and K^2 is the shear correction factor to acknowledge the fact that transverse shear strains are not independent of the thickness coordinate. Also, $\nu_1 = (1 - \nu)/2$ and $\nu_2 = (1 + \nu)/2$ where ν is Poisson's ratio, and $\psi_{k,ij}$ is $\frac{\partial^2 \psi_k}{\partial i \partial j}$. In the Eqs. (1) comma-subscript convention represents the partial derivatives with respect to the normalized coordinates (X_1, X_2, X_3) . $\tilde{\psi}_3$ is non-dimensional transverse displacement, $\tilde{\psi}_1$ and $\tilde{\psi}_2$ are non-dimensional slope due to bending alone in the respective planes which are defined by the following relations,

$$\tilde{\psi}_1(X_1, X_2) = \psi_1(x_1, x_2, t) e^{-i\omega t}, \quad (2a)$$

$$\tilde{\psi}_2(X_1, X_2) = \psi_2(x_1, x_2, t) e^{-i\omega t}, \quad (2b)$$

$$\tilde{\psi}_3(X_1, X_2) = \psi_3(x_1, x_2, t) e^{-i\omega t} / a \quad (2c)$$

where t is time, ω is the frequency parameter, X_1 and X_2 are dimensionless coordinates defined as $X_1 = \frac{x_1}{a}$, $X_2 = \frac{x_2}{b}$. The displacements along the x_1 and x_2 axes are denoted by u and v respectively, while displacement in the direction of non-deformed middle surface is denoted by w .

In Mindlin plate theory[8], the displacement components are assumed to be given as:

$$u = -x_3 \psi_1(x_1, x_2, t) \quad (3a)$$

$$v = -x_3 \psi_2(x_1, x_2, t) \quad (3b)$$

$$w = \psi_3(x_1, x_2, t) \quad (3c)$$

The resultant bending moments, twisting moments, and the transverse shear forces in dimensionless form are:

$$\tilde{M}_{11} = -(\tilde{\psi}_{1,1} + v\eta\tilde{\psi}_{2,2})e^{i\omega t} \quad (4a)$$

$$\tilde{M}_{22} = -(\eta\tilde{\psi}_{2,2} + v\tilde{\psi}_{1,1})e^{i\omega t} \quad (4b)$$

$$\tilde{M}_{12} = \tilde{M}_{21} = -v_1(\eta\tilde{\psi}_{1,2} + \tilde{\psi}_{2,1})e^{i\omega t} \quad (4c)$$

$$\tilde{Q}_1 = -(\tilde{\psi}_1 - \tilde{\psi}_{3,1})e^{i\omega t} \quad (4d)$$

$$\tilde{Q}_2 = -(\tilde{\psi}_2 - \eta\tilde{\psi}_{3,2})e^{i\omega t} \quad (4e)$$

where \tilde{M}_{11} and \tilde{M}_{22} are the bending moments, \tilde{M}_{12} is the twisting moment and \tilde{Q}_1 and \tilde{Q}_2 are shear forces, all per unit length. Three types of classical boundary conditions are presented classified for an edge parallel to the X_2 -normalized axis in Table 1.

2.2 Wave propagation method

From wave point of view, free vibration of any subject can be considered as waves which are traveling along the body. At boundaries, some parts of these propagating waves are reflected in different types of waves, and the rest will be dissipated or transmitted to the neighbors. In order to use WPM method, we must write the governing equation of the motion and boundary conditions in matrix form. Consider the free vibration problem when no external load is applied to the plate. Three dimensionless functions $\tilde{\psi}_1$, $\tilde{\psi}_2$ and $\tilde{\psi}_3$ may be represented in terms of three dimensionless potentials Ψ_1 , Ψ_2 and Ψ_3 as follows [24]:

$$\tilde{\psi}_1 = C_1\Psi_{1,1} + C_2\Psi_{2,1} - \eta\Psi_{3,2} \quad (5a)$$

$$\tilde{\psi}_2 = C_1 \eta \Psi_{1,2} + C_2 \eta \Psi_{2,2} + \Psi_{3,1} \quad (5b)$$

$$\tilde{\psi}_3 = \Psi_1 + \Psi_2 \quad (5c)$$

where parameters C_1 and C_2 are $C_1 = 1 - \frac{\alpha_2^2}{v_1 \alpha_3^2}$, $C_2 = 1 - \frac{\alpha_1^2}{v_1 \alpha_3^2}$. Also, α_1, α_2 and α_3 can be obtained from Eqs. (5) as follows:

$$\alpha_1^2, \alpha_2^2 = \frac{\beta^2}{2} \left[\frac{\delta^2}{12} \left(\frac{1}{K^2 v_1} + 1 \right) \mp \sqrt{\left(\frac{\delta^2}{12} \right)^2 \left(\frac{1}{K^2 v_1} - 1 \right)^2 + \frac{4}{\beta^2}} \right], \quad (6a)$$

$$\alpha_3^2 = \frac{12K^2}{\delta^2 \beta^2} \alpha_1^2 \alpha_2^2 = \frac{12K^2}{\delta^2} \left(\frac{\beta^2 \delta^4}{144K^2 v_1} - 1 \right) \quad (6b)$$

By substituting Eqs. (5) into Eqs. (1), three coupled equations of motion will be uncoupled in terms of potential parameters as:

$$\Psi_{1,11} + \eta^2 \Psi_{1,22} = -\alpha_1^2 \Psi_1 \quad (7a)$$

$$\Psi_{2,11} + \eta^2 \Psi_{2,22} = -\alpha_2^2 \Psi_2 \quad (7b)$$

$$\Psi_{3,11} + \eta^2 \Psi_{3,22} = -\alpha_3^2 \Psi_3 \quad (7c)$$

Considering that two opposite-side edges are simply-supported at $X_1 = 0$ and $X_1 = 1$, the solution for Eqs. (7) can be obtained as:

$$\Psi_1 = [A_1 \sin(\lambda_1 X_2) + A_2 \cos(\lambda_1 X_2)] \sin(m\pi X_1) \quad (8a)$$

$$\Psi_2 = [A_3 \sinh(\lambda_2 X_2) + A_4 \cosh(\lambda_2 X_2)] \sin(m\pi X_1) \quad (8b)$$

$$\Psi_3 = [A_5 \sinh(\lambda_3 X_2) + A_6 \cosh(\lambda_3 X_2)] \cos(m\pi X_1) \quad (8c)$$

where A_i are arbitrary constants. The dispersion relation for these set of solutions is calculated in terms of α_i :

$$\alpha_1^2 = (m\pi)^2 + \eta^2 \lambda_1^2, \quad \alpha_2^2 = (m\pi)^2 - \eta^2 \lambda_2^2, \quad \alpha_3^2 = (m\pi)^2 - \eta^2 \lambda_3^2 \quad (9)$$

Substituting Eqs. (8) using Eqs. (5), and by doing some calculations, $\check{\psi}_1, \check{\psi}_2$ and $\check{\psi}_3$ can be redefined as:

$$\check{\psi}_1 = [A'_1 C_1 m\pi e^{i\lambda_1 X_2} + A'_2 C_1 m\pi e^{-i\lambda_1 X_2} + A'_3 C_2 m\pi e^{\lambda_2 X_2} + A'_4 C_2 m\pi e^{-\lambda_2 X_2} + A'_5 \eta \lambda_3 e^{\lambda_3 X_2} + A'_6 \eta \lambda_3 e^{-\lambda_3 X_2}] \cos(m\pi X_1) \quad (10a)$$

$$\check{\psi}_2 = [A'_1 C_1 \eta \lambda_1 e^{i\lambda_1 X_2} + A'_2 C_1 \eta \lambda_1 e^{-i\lambda_1 X_2} + A'_3 C_2 \eta \lambda_2 e^{\lambda_2 X_2} + A'_4 C_2 \eta \lambda_2 e^{-\lambda_2 X_2} + A'_5 m\pi e^{\lambda_3 X_2} + A'_6 m\pi e^{-\lambda_3 X_2}] \sin(m\pi X_1) \quad (10b)$$

$$\check{\psi}_3 = [A''_1 e^{i\lambda_1 X_2} + A''_2 e^{-i\lambda_1 X_2} + A''_3 e^{\lambda_2 X_2} + A''_4 e^{-\lambda_2 X_2}] \sin(m\pi X_1) \quad (10c)$$

Undefined amplitude parameters in the first equation of Eq. (10a) are:

$$A'_1 = \frac{-iA_1 + A_2}{2}, A'_2 = \frac{iA_1 + A_2}{2}, A'_3 = \frac{A_3 + A_4}{2} \quad (11a)$$

$$A'_4 = \frac{-A_3 + A_4}{2}, A'_5 = \frac{-A_5 - A_6}{2}, A'_6 = \frac{-A_5 + A_6}{2}$$

For the coefficients of other two equations in the Eqs. (10), the following relations are detected:

$$A''_1 = iA'_1, \quad A''_2 = -iA'_2, \quad A''_3 = A'_3 \quad (11b)$$

$$A''_4 = -A'_4, \quad A''_5 = A'_5, \quad A''_6 = -A'_6$$

$$A'''_1 = A'_1, \quad A'''_2 = A'_2, \quad A'''_3 = A'_3, \quad A'''_4 = A'_4$$

These relations help to rewrite all Eqs. (10) with the same coefficients for all of them. Using Eq. (11b), the rewritten form of Eqs. (10) would be:

$$\check{\psi}_1 = [A'_1 C_1 m\pi e^{i\lambda_1 X_2} + A'_2 C_1 m\pi e^{-i\lambda_1 X_2} + A'_3 C_2 m\pi e^{\lambda_2 X_2} + A'_4 C_2 m\pi e^{-\lambda_2 X_2} + A'_5 \lambda_3 \eta e^{\lambda_3 X_2} + A'_6 \lambda_3 \eta e^{-\lambda_3 X_2}] \cos(m\pi X_1) \quad (12a)$$

$$\begin{aligned} \tilde{\psi}_2 = & [A'_1 i C_1 \lambda_1 \eta e^{i\lambda_1 X_2} - A'_2 i C_1 \lambda_1 \eta e^{-i\lambda_1 X_2} + A'_3 C_2 \lambda_2 \eta e^{\lambda_2 X_2} - A'_4 C_2 \lambda_2 \eta e^{-\lambda_2 X_2} + A'_5 m \pi e^{\lambda_3 X_2} \\ & - A'_6 m \pi e^{-\lambda_3 X_2}] \sin(m \pi X_1) \end{aligned} \quad (12b)$$

$$\tilde{\psi}_3 = [A'_1 e^{i\lambda_1 X_2} + A'_2 e^{-i\lambda_1 X_2} + A'_3 e^{\lambda_2 X_2} + A'_4 e^{-\lambda_2 X_2}] \sin(m \pi X_1) \quad (12c)$$

In Eqs. (12), there are six traveling waves detected in the plate, three positive- and three negative-going waves traveling in X_2 direction with different wave numbers λ_i . The positive- and negative-going waves are defined as bellow:

$$\mathbf{a}^+(x) = \begin{pmatrix} A'_2 e^{-i\lambda_1 X_2} \\ A'_4 e^{-\lambda_2 X_2} \\ A'_6 e^{-\lambda_3 X_2} \end{pmatrix}, \quad \mathbf{a}^-(x) = \begin{pmatrix} A'_1 e^{i\lambda_1 X_2} \\ A'_3 e^{\lambda_2 X_2} \\ A'_5 e^{\lambda_3 X_2} \end{pmatrix} \quad (13a,b)$$

In which $\mathbf{a}^+(x)$ and $\mathbf{a}^-(x)$ are positive and negative-going waves traveling along X_2 direction ,respectively as shown in Fig.1. The first waves in Eqs. (13a,b) are considered generally to be propagating waves, and the next two waves with λ_2 and λ_3 wavenumbers are attenuating waves.

2.3 Propagation and reflection matrices

Consider two points on a vibrating plate a distance X_0 apart in X_2 direction as shown in Fig. 2. Positive- and negative-going waves propagate from one point to another. Denoting them as Eqs. (13), they are related by:

$$\mathbf{a}^+(X + X^0) = \mathbf{f}^+(X) \mathbf{a}^+(X^0), \quad \mathbf{a}^-(X^0) = \mathbf{f}^-(X) \mathbf{a}^-(X + X^0) \quad (14a,b)$$

where $X^0 = (X_1^0, X_2^0, X_3^0)$ is an arbitrary point on the plate, $X = (X_1, X_2, X_3)$ is the position of any point relative to X^0 in X_2 direction, and $\mathbf{f}^+(X), \mathbf{f}^-(X)$ are propagation matrices in positive and negative directions, respectively. By using Eqs. (13) and (14), we can derive the propagation matrices as bellow:

$$\mathbf{f}^+(X) = \mathbf{f}^-(X) = \begin{bmatrix} e^{-i\lambda_1 X_2} & 0 & 0 \\ 0 & e^{-\lambda_2 X_2} & 0 \\ 0 & 0 & e^{-\lambda_3 X_2} \end{bmatrix} \quad (15)$$

From wave point of view, free vibration of any subject can be considered as waves which are traveling along the body. At boundaries, the incident wave \mathbf{a}^+ gives rise to the reflected wave \mathbf{a}^- , which are related by [27]

$$\mathbf{a}^- = \mathbf{r}\mathbf{a}^+ \quad (16)$$

The \mathbf{a}^+ and \mathbf{a}^- are positive- and negative-going waves respectively, and \mathbf{r} is reflection matrix. In order to find the reflection matrices. We will find the reflection matrix for simply supported, clamped, and free boundary conditions.

The equilibrium conditions for the simply supported boundary condition from Table 1 are:

$$\tilde{M}_{22} = 0, \quad \check{\psi}_1 = 0, \quad \check{\psi}_3 = 0 \quad (17)$$

By using Eqs. (4), (12), (13), and (17) and doing some calculations, it results in:

$$\begin{aligned} & [-C_1\lambda_1^2\eta^2 - C_1(m\pi)^2\nu]a_1^+ + [C_2\lambda_2^2\eta^2 - C_2(m\pi)^2\nu]a_2^+ + [m\pi\eta\lambda_3 - \lambda_3\eta m\pi\nu]a_3^+ + \\ & [-C_1\lambda_1^2\eta^2 - C_1(m\pi)^2\nu]a_1^- + [C_2\lambda_2^2\eta^2 - C_2(m\pi)^2\nu]a_2^- + [m\pi\eta\lambda_3 - \eta\lambda_3 m\pi\nu]a_3^- = 0 \end{aligned} \quad (18a)$$

$$C_1 m\pi a_1^+ + C_2 m\pi a_2^+ + \eta\lambda_3 a_3^+ + C_1 m\pi a_1^- + C_2 m\pi a_2^- + \eta\lambda_3 a_3^- = 0 \quad (18b)$$

$$a_1^+ + a_2^+ + a_1^- + a_2^- = 0 \quad (18c)$$

By rewriting Eqs. (18) in a matrix form as Eq. (16), one gets:

$$\mathbf{r}_s = -\mathbf{I} \quad (19)$$

where \mathbf{r}_s is the reflection matrix for simply supported boundary condition, “I” is 3×3 identity matrix.

In clamped boundary condition, the equilibrium conditions at the boundary are (Table 1):

$$\check{\psi}_1 = 0, \quad \check{\psi}_2 = 0, \quad \check{\psi}_3 = 0 \quad (20)$$

Substituting Eqs. (12) into Eq. (20), with respect to Eqs. (13) yields

$$C_1 m \pi a_1^+ + C_2 m \pi a_2^+ + \eta \lambda_3 a_3^+ + C_1 m \pi a_1^- + C_2 m \pi a_2^- + \eta \lambda_3 a_3^- = 0 \quad (21a)$$

$$-i C_1 \lambda_1 \eta a_1^+ - C_2 \lambda_2 \eta a_2^+ - m \pi a_3^+ + i C_1 \lambda_1 \eta a_1^- + C_2 \lambda_2 \eta a_2^- + m \pi a_3^- = 0 \quad (21b)$$

$$a_1^+ + a_2^+ + a_1^- + a_2^- = 0 \quad (21c)$$

By rewriting Eqs. (21) in a matrix form as Eq. (16), one obtains:

$$\mathbf{r}_c = - \begin{bmatrix} C_1 m \pi & C_2 m \pi & \eta \lambda_3 \\ -i C_1 \lambda_1 \eta & -C_2 \lambda_2 \eta & -m \pi \\ 1 & 1 & 0 \end{bmatrix}^{-1} \begin{bmatrix} C_1 m \pi & C_2 m \pi & \eta \lambda_3 \\ i C_1 \lambda_1 \eta & C_2 \lambda_2 \eta & m \pi \\ 1 & 1 & 0 \end{bmatrix} \quad (22)$$

where \mathbf{r}_c is the reflection matrix for the clamped boundary condition. After some mathematical calculations and simplifications, the components of the reflection matrix for clamped boundary condition can be determined as:

$$r_c(1,1) = \{c_2[(m\pi)^2 - \eta^2 \lambda_2 \lambda_3] + c_1[-(m\pi)^2 - i\eta^2 \lambda_1 \lambda_3]\}/\Sigma \quad (23a)$$

$$r_c(1,2) = -2c_2 \eta^2 \lambda_2 \lambda_3 / \Sigma \quad (23b)$$

$$r_c(1,3) = -2m\pi \eta \lambda_3 / \Sigma \quad (23c)$$

$$r_c(2,1) = 2ic_1 \eta^2 \lambda_1 \lambda_3 / \Sigma \quad (23d)$$

$$r_c(2,2) = \{c_2[(m\pi)^2 + \eta^2 \lambda_2 \lambda_3] - c_1[(m\pi)^2 - i\eta^2 \lambda_1 \lambda_3]\}/\Sigma \quad (23e)$$

$$r_c(2,3) = 2m\pi \eta \lambda_3 / \Sigma \quad (23f)$$

$$r_c(3,1) = 2im\pi c_1 \eta \lambda_1 (c_1 - c_2) / \Sigma \quad (23g)$$

$$r_c(3,2) = 2m\pi c_2 \eta \lambda_2 (c_1 - c_2) / \Sigma \quad (23h)$$

$$r_c(3,3) = \{-c_2[(m\pi)^2 + \eta^2 \lambda_2 \lambda_3] + c_1[(m\pi)^2 + i\eta^2 \lambda_1 \lambda_3]\}/\Sigma \quad (23j)$$

where $r_c(i,j)$ is the element in i-th row and j-th column, and Σ is a parameter defined for the sake of simplicity and it is equal to:

$$\Sigma = c_2[-(m\pi)^2 + \eta^2 \lambda_2 \lambda_3] + c_1[(m\pi)^2 - i\eta^2 \lambda_1 \lambda_3] \quad (24)$$

Finally, for free boundary conditions, the equilibrium conditions from Table 1 are:

$$\tilde{M}_{22} = 0, \quad \tilde{M}_{21} = 0, \quad \tilde{Q}_2 = 0, \quad (25)$$

Substituting Eqs.(12) into Eq. (25), and with respect to Eqs. (13), (13) yields:

$$\begin{aligned} & [-C_1 \lambda_1^2 \eta^2 - C_1 (m\pi)^2 \nu] a_1^+ + [C_2 \lambda_2^2 \eta^2 - C_2 (m\pi)^2 \nu] a_2^+ + [m\pi \eta \lambda_3 - \lambda_3 \eta m\pi \nu] a_3^+ \\ & + [-C_1 \lambda_1^2 \eta^2 - C_1 (m\pi)^2 \nu] a_1^- + [C_2 \lambda_2^2 \eta^2 - C_2 (m\pi)^2 \nu] a_2^- \\ & + [m\pi \eta \lambda_3 - \eta \lambda_3 m\pi \nu] a_3^- = 0 \end{aligned} \quad (26a)$$

$$\begin{aligned} & -2iC_1 \lambda_1 \eta m\pi a_1^+ - 2C_2 \lambda_2 \eta m\pi a_2^+ + [-\lambda_3^2 \eta^2 - (m\pi)^2] a_3^+ + 2iC_1 \lambda_1 \eta m\pi a_1^- \\ & + 2C_2 \lambda_2 \eta m\pi a_2^- + [\lambda_3^2 \eta^2 + (m\pi)^2] a_3^- = 0, \end{aligned} \quad (26b)$$

$$\begin{aligned} & (-iC_1 \lambda_1 \eta + i\lambda_1 \eta) a_1^+ + (-C_2 \lambda_2 \eta + \lambda_2 \eta) a_2^+ - m\pi a_3^+ + (iC_1 \lambda_1 \eta - i\lambda_1 \eta) a_1^- \\ & + (C_2 \lambda_2 \eta - \lambda_2 \eta) a_2^- + m\pi a_3^- = 0, \end{aligned} \quad (26c)$$

Eqs. (26) can be written in a matrix form as $\mathbf{a}^- = \mathbf{r} \mathbf{a}^+$:

$$\begin{aligned} \mathbf{r}_F = & - \begin{bmatrix} -C_1 \lambda_1^2 \eta^2 - C_1 (m\pi)^2 \nu & C_2 \lambda_2^2 \eta^2 - C_2 (m\pi)^2 \nu & m\pi \eta \lambda_3 - \lambda_3 \eta m\pi \nu \\ -2iC_1 \lambda_1 \eta m\pi & -2C_2 \lambda_2 \eta m\pi & -\lambda_3^2 \eta^2 - (m\pi)^2 \\ -iC_1 \lambda_1 \eta + i\lambda_1 \eta & -C_2 \lambda_2 \eta + \lambda_2 \eta & -m\pi \end{bmatrix}^{-1} \times \\ & \begin{bmatrix} -C_1 \lambda_1^2 \eta^2 - C_1 (m\pi)^2 \nu & C_2 \lambda_2^2 \eta^2 - C_2 (m\pi)^2 \nu & m\pi \eta \lambda_3 - \eta \lambda_3 m\pi \nu \\ 2iC_1 \lambda_1 \eta m\pi & 2C_2 \lambda_2 \eta m\pi & \lambda_3^2 \eta^2 + (m\pi)^2 \\ iC_1 \lambda_1 \eta - i\lambda_1 \eta & C_2 \lambda_2 \eta - \lambda_2 \eta & m\pi \end{bmatrix} \end{aligned} \quad (27)$$

where \mathbf{r}_F is the reflection matrix for free boundary condition. In order to analyze the vibration systemically, we need to use Eqs, (14), (16) and, the obtained propagation and reflection matrices. In this way, we will be able to analyze the frequency response of the system by solving the following equation:

$$\begin{bmatrix} -\mathbf{I}_{3 \times 3} & \mathbf{r}_A & \mathbf{0} & \mathbf{0} \\ \mathbf{f}^+ & \mathbf{0} & -\mathbf{I}_{3 \times 3} & \mathbf{0} \\ \mathbf{0} & -\mathbf{I}_{3 \times 3} & \mathbf{0} & \mathbf{f}^- \\ \mathbf{0} & \mathbf{0} & \mathbf{r}_B & -\mathbf{I}_{3 \times 3} \end{bmatrix} \begin{bmatrix} \mathbf{a}^+ \\ \mathbf{a}^- \\ \mathbf{b}^+ \\ \mathbf{b}^- \end{bmatrix} = 0 \quad (28)$$

where \mathbf{a} and \mathbf{b} are the positive- and negative-going waves at two opposite boundaries as shown in Fig.1. By setting the imaginary and real parts of the determinant of Eq. (28), which is the familiar characteristic equation for the Mindlin plate, for simply supported, clamped and free boundary conditions, the resonant frequencies of each of the mentioned boundary conditions will be obtained.

3. Numerical results and discussion

3.1 Validation of the present method

In order to investigate the accuracy and reliability of this study, present results are compared with literature. Table 2 presents the comparison study of the fundamental non-dimensional natural frequency of the present work with [5], [19], [23], [22], and [24] for different boundary conditions, thickness to length ratio, and aspect ratio of the plate. For defining different boundary conditions at edges symbolisms are considered, for example, SCSF indicates that the edges $x_1 = 0, x_2 = 0, x_1 = a$, and $x_2 = b$ are simply-supported, clamped, simply-supported and free, respectively. For comparison, the following material and geometrical properties are considered: shear correction factor, $K^2 = 0.86667$; Young's modulus, $E = 1$ TPa; shear modulus, $G = E / [2(1 + \nu)]$; Poisson's ratio $\nu = 0.3$; the rectangular plate is considered to be square and non-square by using two different aspect ratios ($\eta = 1, 0.4$); thickness to length ratio is investigated for four different values ($\delta = 0.001, 0.01, 0.1, 0.2$). Values n and m show that the vibrating mode has n and m half-waves in the x_1 and x_2 directions, respectively; their values are considered to be ($m = 1, n = 1$)

for the comparison of the first mode shape. Among the aforementioned references, [5] and [24] have used exact characteristic equation for thin and thick plates respectively; alternatively, [19], [23], and [22] have implemented approximate solutions. Leissa's well-known paper [5] proposed exact characteristic equation for thin plates, so in order to compare present results with available data in his paper, the value for thickness to length ratio is considered to be $\delta = 0.001$ in $\eta = 1$ case and $\delta = 0.01$ in $\eta = 0.4$ case. Another way of comparing the present results with the results of thin plate is by taking into account the relevant assumptions for thin plates in which one of them would be letting $K^2 \rightarrow \infty$. The results for exact characteristic equations for thick plates available in [24] are compared with exact results of the present work and as it is seen that they show precise agreement. The results are also in good agreement with approximate solutions of [19], [23], and [22] where the two dimensional Ritz method and boundary characteristic orthogonal polynomials along with three dimensional Ritz method was implemented, respectively. The point for the latter comparison is that the shear correction factor employed in the present study, [24] and [22] is $K^2 = 0.86667$, in [19] is $K^2 = 5/6$, and in [23] is assumed to be $K^2 = \pi/12$. This affects the results slightly.

3.2 Frequency calculation

The non-dimensional natural frequencies can be calculated using the present method as illustrated in Fig. 3 for a plate with SCSC boundary conditions, thickness to length ratio $\delta = 0.15$, aspect ratio $\eta = 0.6$, shear correction factor $K^2 = 0.86667$, Poisson's ratio $\nu = 0.3$, and $m=1$. As shown in Fig. 3, in the wave propagation method, for evaluating the natural frequencies, the real and imaginary curves of determinant of Eq. (28) should meet zero simultaneously. It should be

mentioned that in this figure the first point where imaginary and real parts meet zero simultaneously is not a natural frequency, yet it is a cut-off frequency where the type of waves changes to another one. The first point after cut-off frequency where both imaginary and real parts meet zero is the fundamental natural frequency in x_2 - direction ($n=1$) and the second point is the second natural frequency in that direction ($n=2$) and so forth.

The Cut-off frequencies (COF) are frequencies where the type of wave changes for frequencies below and above them. In this study, two types of waves are detected; attenuating waves and propagating waves. There are three positive- and negative-going waves in x_2 direction defined by Eq. (13). It is obvious that if λ_1 is real, the first wave will be a propagating wave; otherwise, it is an attenuating wave. Besides, if λ_2 and λ_3 are real or imaginary, the second and the third type of waves will be attenuating or propagating waves, respectively. Fig. 4 depicts the dispersion relations given by Eq. (9) where the relation between wavenumbers and the frequency is presented. The material and geometrical properties are considered as aforementioned properties. In Fig. 4, three cut-off frequencies are detectable where at each COF, the type of one wave changes. It is noticeable that at low frequencies there are only attenuating waves and at high frequencies there are only propagating waves. At each COF, one of the waves converts to another type; all three times from an attenuating wave to a propagating wave, so after three COFs, all attenuating waves convert to propagating waves.

Table 3 presents the frequency benchmark results for different boundary conditions, aspect ratios, thickness to length ratios, and different numbers of half waves in each direction. The results are obtained for SCSC, SCSS, SSSS, SCSF, SFSS, SFSF boundary conditions. The aspect ratio is considered to have different values of $\eta = 0.6, 0.8, 1, 1.5, 2$, and the thickness to length ratio is considered to be $\delta = 0.01, 0.1, 0.2$. Also, the natural frequency is given for four different mode

numbers $((m,n)=(1,1), (1,2), (2,1), (2,2))$. These results are regarded as the exact results for thick plate so they are an excellent database for future works.

From the results presented in Table 3, it can be observed that the lowest natural frequencies correspond to the plate subjected to less edge restraints. As the number of edge restraint increases, the natural frequency parameters also increase. Among all six combinations of the boundary conditions listed in Table 3, it can be seen that the lowest and highest values of the frequency parameters correspond to S–F–S–F and S–C–S–C cases, respectively. Moreover, increasing both values of the thickness to length ratio (δ) and aspect ratio ($1/\eta$) result in a decrease in natural frequency in every mode shapes and boundary conditions.

3.3 Reflection analysis of waves in Mindlin plates

Waves which are incident upon boundaries may reflect in different types of waves. There are three waves of two different types traveling in a thick plate based on first order shear deformation theory. The power carried in a propagating wave is proportional to the square of the wave amplitude. Thus, the power reflected per unit incident power can be calculated by the square of the reflection coefficients $|r_{ij}|^2$ [27]. So, it is possible to calculate the reflected power at boundaries by investigating the behavior of the reflection coefficients. Coefficients of reflection matrix can be viewed from a different perspective. The j -th column of the reflection matrices represents the reflection contribution of the j -th incident wave in 1st, 2nd, ..., i -th reflected waves while the i -th row of the reflection matrices represents the reflection contribution of 1st, 2nd, ..., j -th incident waves in the i -th reflected wave. In other words, r_{ij} represents the reflection contribution of the j -th incident wave in the i -th reflected wave. The mechanical properties of the plate is considered as the previous section. It is shown that reflection coefficients generally depend on five parameters

and they are independent of the aspect ratio of the plate, so the position of the boundaries is unimportant. The COFs has significant effects on the moduli of reflection coefficients as at these frequencies, the type of waves changes; they are distinctly visible in reflection coefficients graphs. The thickness to length ratio of the plate has substantial effects on the behavior of the reflection coefficients and this effect is investigated. There are two physical boundary conditions considered namely clamped, and simply-supported boundary conditions. Different boundary conditions show different responses to incident waves in which the reflected power varies from one boundary condition to another one, so for each of these two classical boundary conditions, the results are discussed and investigated separately. It is observed that a specific type of incident wave may induce reflected waves of other types, and these phenomena profoundly depend on the type of the boundary condition and frequency parameter.

3.3.1 Reflection coefficients for simply supported boundary conditions

As it can be seen by Eq. (19), the reflection coefficients for simply supported edge are constant and they are independent of five parameters m , δ , K , β , and ν . In other words, if a propagating wave alone or an attenuating wave alone is incident upon the simply supported boundary, no energy will dissipate and the reflected power of the same type of incident wave is the same as the incident wave power. Furthermore, if a propagating wave or an attenuating wave alone is incident upon the simply supported boundary, exclusively the same type of wave will be reflected and there will not be any other types of reflected waves. In other words, if a propagating wave alone is incident upon the simply supported boundary, there will not be any attenuating wave in the reflected wave. This is due to the fact that the reflection matrix has zero off-diagonal components.

3.3.2 Reflection coefficients for clamped boundary conditions

For simplification, we divided the frequency range into four regions; $0 < \beta < \beta_{c1}$, $\beta_{c1} < \beta < \beta_{c2}$, $\beta_{c2} < \beta < \beta_{c3}$, and $\beta > \beta_{c3}$. Subscripts show the cut-off frequencies, for example, β_{c1} shows the first cut-off frequency. In clamped boundary condition, the reflection matrix coefficients depend on m , δ , K , β , and ν as it is clear from Eqs. (23) and (24). In Fig. 5, the moduli of the reflection coefficients $|r_{ij}|$ are depicted in case of clamped boundary conditions for different values of δ . ($\delta = 0.15, 0.175, 0.2, 0.225$).

Three cut-off frequencies are recognizable in this figure where at these frequencies the wave type of each entry of reflection matrix is transformed into a different one causing sharp jumps or drops. It is noticeable from Fig. 5 that the values of these three COFs are dependent on the thickness to length ratio parameter δ . As the thickness to length ratio parameter increases, these three COFs shift to the lower frequencies.

In the first frequency region $0 < \beta < \beta_{c1}$, λ_1 is pure imaginary while λ_2 and λ_3 are real suggesting the existence of three attenuating waves a_1 , a_2 , a_3 . In this frequency range, the moduli of eight reflection coefficients decrease as the frequency parameter increases except for the modulus of reflection coefficient r_{32} where there is a frequency below β_{c1} in which the maximum modulus of reflection coefficient r_{32} occurs. In the first frequency region, increasing the thickness to length ratio leads to reduction in six moduli of the reflection coefficients r_{11} , r_{12} , r_{13} , r_{21} , r_{22} , r_{23} except for r_{31} , r_{32} , r_{33} which increase by increasing the thickness to length ratio δ . In other words, if attenuating waves with λ_1 , λ_2 , λ_3 wavenumbers are incident upon the clamped boundary in the first frequency region, the power of the attenuating reflected wave with λ_3 wavenumber increases with increasing the thickness to length ratio δ .

In the second frequency region between β_{c1} and β_{c2} , λ_1 changes its value from imaginary into real and the other two wavenumbers λ_2, λ_3 remain unchanged. This implies that in the second region $\beta_{c1} < \beta < \beta_{c2}$ there are two attenuating waves a_2, a_3 and one propagating wave a_1 . In this frequency region, the modulus of r_{11} is independent of the frequency and its value is constant and unity. So, if a propagating wave with λ_1 wavenumber is incident upon a clamped boundary condition, the power of the propagating reflected wave with λ_1 wavenumber will be the same as the incident wave power. As shown in Fig. 5, above the first COF, as the frequency parameter increases, the modulus of the reflection coefficient r_{12} increases then, there is a reduction till it reaches zero at the second COF β_{c2} . The moduli of reflection coefficients r_{13} and r_{23} decreases till it reaches zero at the second COF. The modulus of the reflection coefficient r_{21} increases till it reaches a maximum value then, there is a reduction till it reaches zero at the second COF. The modulus of the reflection coefficient r_{22} increases then, there is a reduction till it reaches one at the second COF β_{c2} . In other words, if an attenuating wave with λ_2 wavenumber is incident upon a clamped boundary at the second COF, the power of the attenuating reflected wave with λ_2 wavenumber is equal to the incident wave power. The modulus of the reflection coefficient r_{31} increases from zero then, there is a reduction till it reaches the second COF β_{c2} . The modulus of the reflection coefficient r_{32} increases then, there is a reduction till it reaches the second COF β_{c2} . The modulus of the reflection coefficient r_{33} increases then, there is a reduction till it reaches one at the second COF β_{c2} . In other words, if an attenuating wave with λ_3 wavenumber is incident upon a clamped boundary at the second COF, the power of the attenuating reflected wave with λ_3 wavenumber is equal to the incident wave power. In this frequency range, by increasing the thickness to length ratio, the moduli of all reflection coefficients increase except

r_{13}, r_{23}, r_{11} and r_{21} where there is a reduction in three reflection coefficients r_{13}, r_{23}, r_{21} and the modulus of reflection coefficient r_{11} is independent of the thickness to length ratio.

In the third frequency region $\beta_{c2} < \beta < \beta_{c3}$, λ_3 becomes pure imaginary and the other two wavenumbers λ_1, λ_2 remain unchanged indicating two propagating waves a_1, a_3 and one attenuating wave a_2 . In this frequency region, immediately after β_{c2} , as the frequency parameter increases, the moduli of the reflection coefficients r_{11}, r_{32}, r_{33} decrease while the moduli of the reflection coefficients r_{13}, r_{21}, r_{23} increase till β_{c3} . The situation is different for the reflection coefficients r_{12}, r_{31}, r_{22} . The modulus of reflection coefficient r_{12} increases till it reaches a maximum value then, there is a reduction till it reaches zero at the third COF. The modulus of reflection coefficient r_{31} decreases till it reaches a minimum value then, there is an increase till the third COF. The modulus of reflection coefficient r_{22} is always unity in the third frequency region. In this frequency range, by increasing the thickness to length ratio, the moduli of all reflection coefficients decrease except r_{13}, r_{23}, r_{22} and r_{21} where there is an increase in three reflection coefficients r_{13}, r_{23} and r_{21} and the modulus of reflection coefficient r_{22} is independent of the thickness to length ratio.

In the fourth frequency region $\beta > \beta_{c3}$, above the third COF, λ_2 becomes pure imaginary and the other two wavenumbers λ_1, λ_3 remain unchanged indicating three propagating waves a_1, a_2, a_3 . In this frequency region, as the frequency parameter increases in the fourth region, the moduli of the reflection coefficients $r_{13}, r_{21}, r_{23}, r_{31}, r_{32}$ decrease and asymptote to the value of zero. In other words, the propagating reflected wave power of a propagating incident wave approaches zero in high frequency region. Also, as the frequency parameter increases in the fourth region, the moduli of the reflection coefficients r_{11}, r_{22}, r_{33} increase and asymptote to the value of one. In other words, the propagating reflected wave power of a propagating incident wave is equal to the

incident wave power in high frequency region. Moreover, as the frequency parameter increases in the fourth region, the modulus of the reflection coefficient r_{12} increase and asymptote to the value of two. In other words, if a propagating wave with λ_2 wavenumber a_2^+ is incident upon a clamped boundary, the power of the reflected wave with λ_1 wavenumber a_1^- becomes four times its incident wave power in high frequency region. In this frequency range, by increasing the thickness to length ratio, the moduli of all reflection coefficients increase except $r_{21}, r_{31}, r_{32}, r_{13}, r_{23}$ where there is a reduction in these five reflection coefficients.

4. Conclusion

The wave propagation method is implemented to analyze the energy reflection, propagation, and free vibration of thick plates based on Mindlin plate theory. First of all, the accuracy of the presented method is validated by comparing the obtained resonant frequencies with available literatures. Benchmark results for natural frequencies are presented for various thickness to length ratios, aspect ratios, numbers of half waves, and various combinations of boundary conditions. In future works, these results can be an excellent database to verify approximate or other analytical solutions as they are regarded as exact solutions. The main discussion of the present work is allocated to the investigation of wave power reflection, dissipation and conversion for two physical boundary conditions (clamped, and simply-supported). The 3×3 reflection matrices are obtained for each boundary conditions creating nine reflection elements ($r_{11}, r_{12}, \dots, r_{32}, r_{33}$), four frequency ranges based on three COFs, and three incident waves with λ_1, λ_2 , and λ_3 wavenumbers. For each region, the behavior of these nine arrays in the reflection matrix are determined. The three waves were either attenuating (at low frequencies) or propagating waves (at high frequencies). After each COF, one of the waves is converted to another type and every time from an attenuating wave to a

propagating wave, so after three COFs all three waves change into the propagating waves. This step by step conversion has substantial impact on the response of the plate and energy conduction in the plate. It is shown that how each wave's energy contributes in another type of wave in the process of reflection and one type of wave induces another type of wave. The results show that the reflection from simply supported boundary condition does not depend on the system parameters, but it is dependent on the system parameters in case of clamped boundary conditions.

References

- [1] Ansari R, Shahabodini A, Shojaei MF. Nonlocal three-dimensional theory of elasticity with application to free vibration of functionally graded nanoplates on elastic foundations. *Physica E Low Dimens Syst Nanostruct* 2016;76:70–81.
- [2] Scheuring J. KaiserSelect aerospace product update focusing on thick plate product AA7097. in 27th Advanced Aerospace Materials and Processes (AeroMat) Conference and Exposition 2016.
- [3] Nourisa J, Rouhi G. Biomechanical evaluation of intramedullary nail and bone plate for the fixation of distal metaphyseal fractures. *J Mech Behav Biomed Mater* 2016;56:34–44.
- [4] Senjanović I, Tomić M, Vladimir N, Cho DS. Analytical solution for free vibrations of a moderately thick rectangular plate. *Math Probl Eng* 2013;2013:ID 207460, doi:10.1155/2013/207460.
- [5] Leissa AW. The free vibration of rectangular plates. *J Sound Vib* 1973;31:257–293.
- [6] Senjanović I, Vladimir N, Tomić M. On new first-order shear deformation plate theories. *Mech Res Commun* 2016;73:31–38.
- [7] Reissner E. The effect of transverse shear deformation on the bending of elastic plates. *J Appl Mech T ASME* 1945;12:A69-A77.

- [8] Mindlin RD. Influence of rotary inertia and shear on flexural motions of isotropic elastic plates. *J Appl Mech T ASME* 1951;18:31-38.
- [9] Xiang W, Xing Y. A new first-order shear deformation theory for free vibrations of rectangular plate. *Int J Appl Mech* 2015;7:1550008.
- [10] Endo M. Study on an alternative deformation concept for the Timoshenko beam and Mindlin plate models. *Int J Eng Sci* 2015;87:32–46.
- [11] Senjanović I, Vladimir N, Tomić M. An advanced theory of moderately thick plate vibrations. *J Sound Vib* 2013;332:1868–1880.
- [12] Thai HT, Choi DH. Analytical solutions of refined plate theory for bending, buckling and vibration analyses of thick plates. *Appl Math Model* 2013;37:8310–8323.
- [13] Murty AVK. Higher order theory for vibrations of thick plates. *AIAA* 1977;15:1823–1824.
- [14] Kant T. Numerical analysis of thick plates. *Comput Methods Appl Mech Eng* 1982;31: 1–18.
- [15] Lo KH, Christensen RM, Wu EM. A high-order theory of plate deformation Part 1: Homogeneous plates. *J Appl Mech* 1977;44:663–668.
- [16] Senjanović I, Vladimir N, Cho DS. A new finite element formulation for vibration analysis of thick plates. *Int J Nav Archit Ocean Eng* 2015;7:324–345.
- [17] Falsone G, Settineri D. A Kirchhoff-like solution for the Mindlin plate model: a new finite element approach. *Mech Res Commun* 2012;40:1–10.
- [18] Senjanović I, Vladimir N, Cho DS, Jokić M, Choi TM. Comparative analysis of new shear locking-free finite element with other commonly used approaches in vibration analysis of Mindlin plates. in *1st Pan-American Congress on Computational Mechanics--PANACM 2015, XI Argentine Congress on Computational Mechanics-MECOM 2015*, 2015.
- [19] Liew KM, Xiang Y, Kitipornchai S. Transverse vibration of thick rectangular plates-I. comprehensive sets of boundary conditions. *Comput Struct* 1993;49:1–29.
- [20] Cho DS, Vladimir N, Choi TM. Approximate natural vibration analysis of rectangular plates with openings using assumed mode method. *Int J Nav Archit Ocean Eng* 2013;5:478–491.

- [21] Cho D, Vladimir N, Choi T. Natural vibration analysis of stiffened panels with arbitrary edge constraints using the assumed mode method. *Proc Inst Mech Eng Part M J Eng Marit Environ* 2015;229:340–349.
- [22] Liew KM, Hung KC, Lim MK. Vibration of mindlin plates using boundary characteristic orthogonal polynomials. *J Sound Vib* 1995;182:77–90.
- [23] Liew KM, Hung KC, Lim MK. Three-dimensional vibration of rectangular plates: Effects of thickness and edge constraints. *J Sound Vib* 1995;182:709–727.
- [24] Hashemi SH, Arsanjani M. Exact characteristic equations for some of classical boundary conditions of vibrating moderately thick rectangular plates. *Int J Solids Struct* 2005;42: 819–853.
- [25] Cui XY, Liu GR, Li GY. Analysis of Mindlin-Reissner plates using cell-based smoothed radial point interpolation method. *Int J Appl Mech* 2010;2:653–680.
- [26] Civalek O. Numerical solutions to the free vibration problem of Mindlin sector plates using the discrete singular convolution method. *Int J Struct Stab Dyn* 2009;9:267–284.
- [27] Mace BR. Wave reflection and transmission in beams. *J Sound Vib* 1984;97:237–246.
- [28] Mei C, Mace BR. Wave reflection and transmission in Timoshenko beams and wave analysis of Timoshenko beam structures. *J Vib Acoust* 2005;127: 382–394.
- [29] Bahrami MN, Arani MK, Saleh NR. Modified wave approach for calculation of natural frequencies and mode shapes in arbitrary non-uniform beams. *Sci Iran* 2011;18: 1088–1094.
- [30] Bahrami A, Teimourian A. Study on vibration, wave reflection and transmission in composite rectangular membranes using wave propagation approach. *Meccanica* 2017;52: 231-249.
- [31] Bahrami A, Ilkhani MR, Bahrami MN. Wave propagation technique for free vibration analysis of annular circular and sectorial membranes. *J Vib Control* 2015;21:1866–1872.
- [32] Bahrami A, Teimourian A. Free vibration analysis of composite, circular annular membranes using wave propagation approach. *Appl Math Model* 2015;37:4781-96.
- [33] Bahrami A, Teimourian A. Study on the effect of small scale on the wave reflection in

- carbon nanotubes using nonlocal Timoshenko beam theory and wave propagation approach. *Compos Part B-Eng* 2016;91:492–504.
- [34] Bahrami A, Teimourian A. Nonlocal scale effects on buckling, vibration and wave reflection in nanobeams via wave propagation approach. *Compos Struct* 2015;134:1061–1075.
- [35] Bahrami A. A wave-based computational method for free vibration, wave power transmission and reflection in multi-cracked nanobeams. *Compos Part B-Eng* 2017;120:168-181
- [36] Bahrami A. Free vibration, wave power transmission and reflection in multi-cracked nanorods. *Compos Part B-Eng* 2017;127:53-62
- [37] Bahrami A, Teimourian A. Small scale effect on vibration and wave power reflection in circular annular nanoplates. *Compos Part B-Eng* 2017;109: 214-26.
- [38] Ilkhani MR, Bahrami A, Hosseini-Hashemi SH. Free vibrations of thin rectangular nanoplates using wave propagation approach. *Appl Math Model* 2016;40:1287–1299.

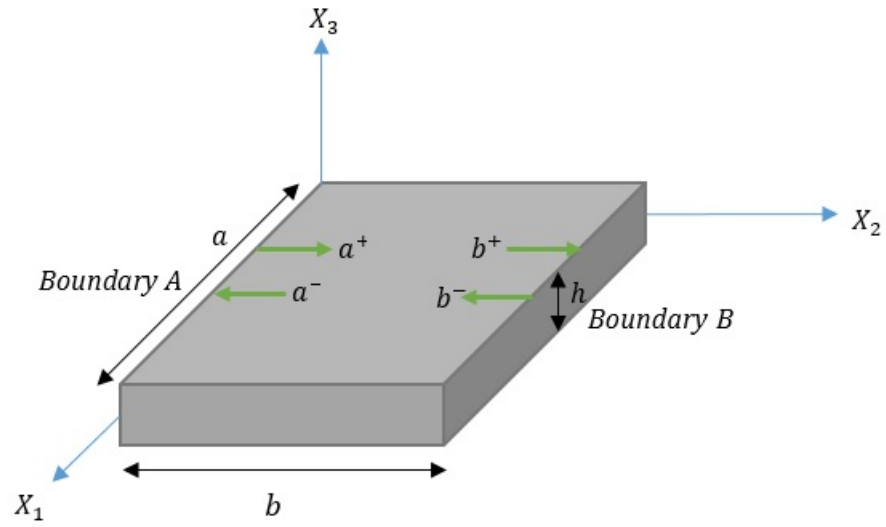


Figure. 1: A Mindlin plate with coordinate convention and waves.

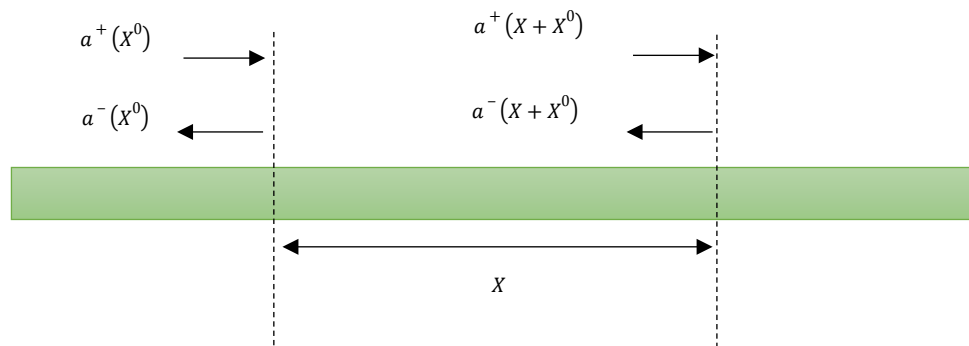


Figure. 2: A lateral view of Mindlin plate representing positive- and negative-going propagating waves.

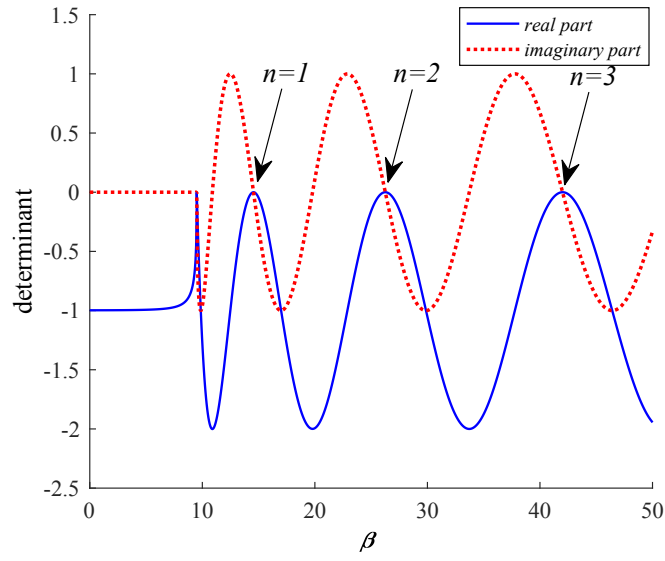


Figure. 3: Real and imaginary parts of determinant of Eq. (28)

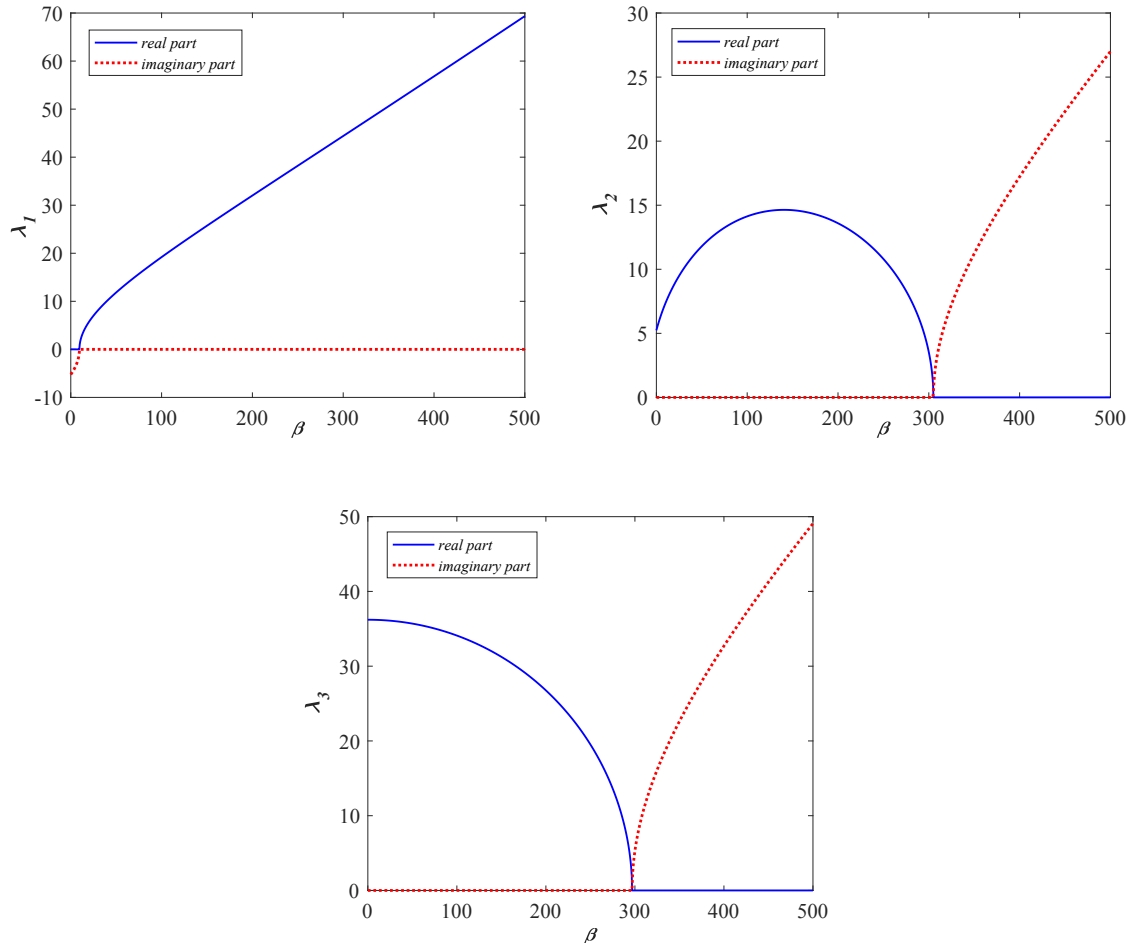
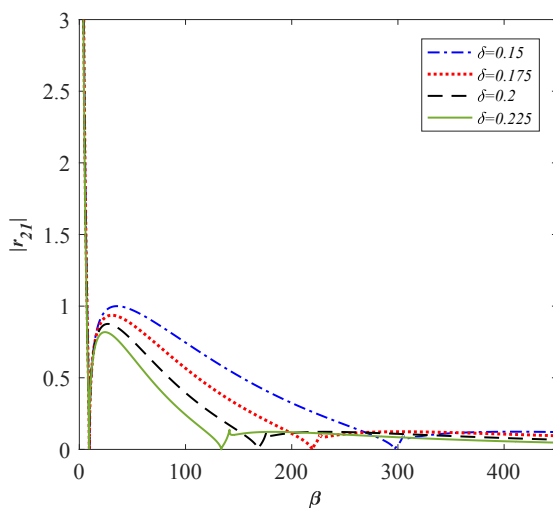
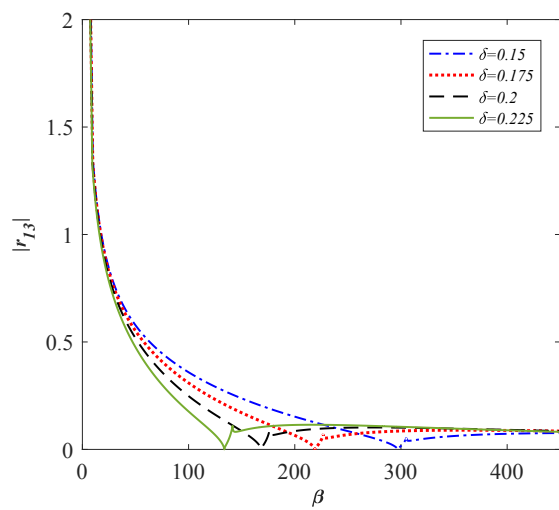
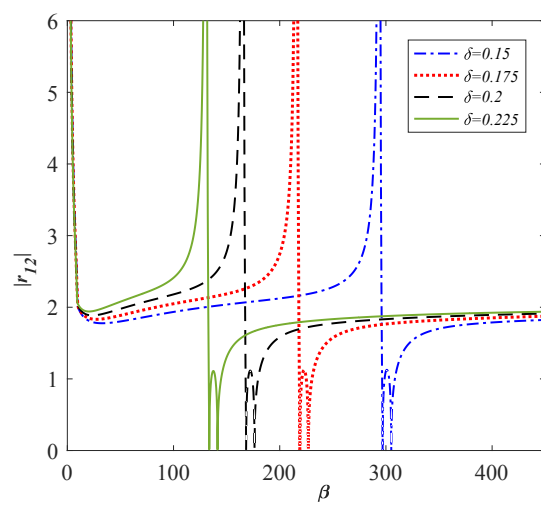
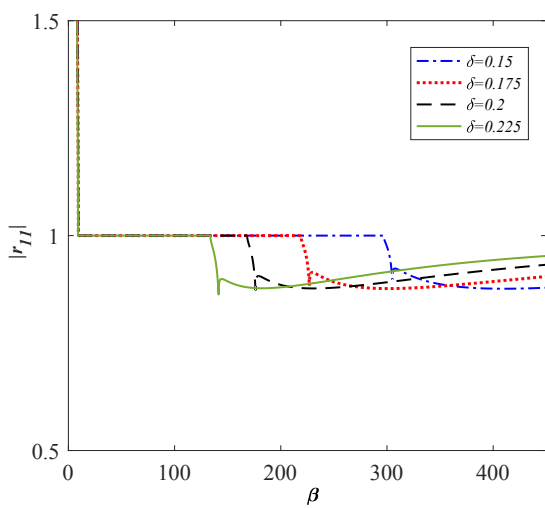


Figure. 4: Wavenumbers against frequency parameter using dispersion relation showing cut off frequencies



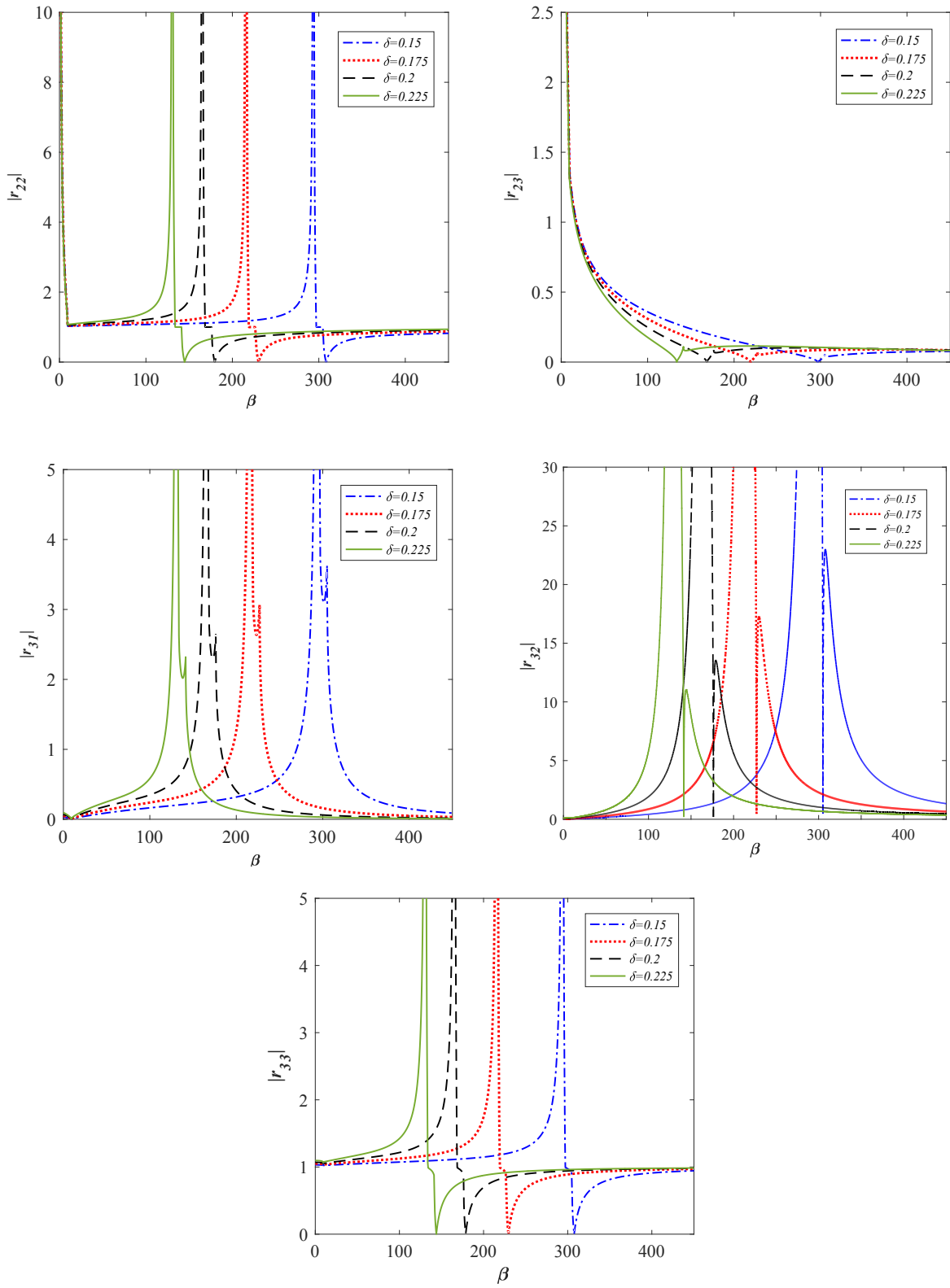


Figure. 5: The moduli of nine reflection coefficients against frequency parameter for different thickness to length ratios in case of clamped boundary condition

Table 1. Equilibrium conditions for different boundary conditions of Mindlin plates

Boundary conditions	Equilibrium conditions
simply-supported edge	$\tilde{M}_{22} = \tilde{\psi}_1 = \tilde{\psi}_3 = 0$
clamped edge	$\tilde{\psi}_1 = \tilde{\psi}_2 = \tilde{\psi}_3 = 0$
free edge	$\tilde{M}_{22} = \tilde{M}_{21} = \tilde{Q}_2 = 0$

Table2 . Comparison of the fundamental frequencies $\beta = \omega a^2 \sqrt{\frac{\rho h}{D}}$ for Mindlin plates with different boundary conditions, aspect ratios, and thickness to length ratios

		Reference	SCSC	SCSS	SSSS	SCSF	SSSF	SFSF
$\eta = 1$	$\delta = 0.001$	Present ^a	28.9505	23.6463	19.7391	12.6862	11.6838	9.6313
		Ref[24] ^a	28.9505	23.6463	19.7391	12.6863	11.6837	9.6311
		Ref[5]	28.9509	23.6463	19.7392	12.6874	11.6845	9.6314
		Ref[19] ^b	28.9515	23.6456	19.7392	12.6854	11.6925	9.6406
		Ref[23] ^c	28.9475	23.6354	19.7392	12.6862	11.6978	9.6327
		Ref[22] ^c	28.9465	23.6325	19.7392	12.6868	11.6981	9.6354
	$\delta = 0.1$	Present ^a	26.7369	22.4260	19.0840	12.2606	11.3808	9.4458
		Ref[24] ^a	26.7369	22.4260	19.0840	12.2606	11.3810	9.4458
		Ref[19] ^b	26.6687	22.4136	19.0651	12.2492	11.3727	9.4403
		Ref[23] ^c	26.6676	22.4336	19.898	12.2546	11.3789	9.4354
		Ref[22] ^c	26.6693	22.4365	19.0582	12.2573	11.3797	9.4462
	$\delta = 0.2$	Present ^a	22.5099	19.7988	17.5055	11.3931	10.7218	8.9997
		Ref[24] ^a	22.5099	19.7988	17.5055	11.3931	10.7218	9.9998
		Ref[19] ^b	22.3596	19.7037	17.4485	11.3619	10.6987	8.9833
		Ref[23] ^c	22.4687	19.7348	17.5264	11.3765	10.7056	9.0010
		Ref[22] ^c	22.4569	19.7389	17.5351	11.3731	10.7102	9.0126
$\eta = 0.4$	$\delta = 0.01$	Present ^a	12.1316	11.7476	11.4464	10.1852	10.1222	9.7572
		Ref[24] ^a	12.1316	11.7476	11.4464	10.1848	10.1222	9.7569
		Ref[5]	12.1347	11.7502	11.4487	10.1888	10.1259	9.7600
		Ref[19] ^b	12.1334	11.7554	11.4501	10.1854	10.1235	9.7583
		Ref[22] ^c	12.1328	11.7556	11.4508	10.1862	10.1238	9.7591
	$\delta = 0.1$	Present ^a	11.8438	11.4978	11.2261	9.9876	9.9311	9.5816
		Ref[24] ^a	11.8438	11.4978	11.2260	9.9871	9.9310	9.5814
		Ref[19] ^b	11.8465	11.5026	11.2265	9.0008	9.9323	9.5832
		Ref[22] ^c	11.8456	11.5048	11.2235	9.0012	9.9324	9.5838
	$\delta = 0.2$	Present ^a	11.1138	10.8485	10.6308	9.4910	9.4472	9.1314
		Ref[24] ^a	11.1138	10.8485	10.6307	9.4910	9.4470	9.1313
		Ref[19] ^b	11.1142	10.8498	10.6318	9.9425	9.44.85	9.1324

^a Shear correction factor $K^2 = 0.86667$

^b Shear correction factor $K^2 = 5/6$

^c Shear correction factor $K^2 = \pi^2/12$

Table3 . Natural frequencies, $\beta = \omega a^2 \sqrt{\frac{\rho h}{D}}$ for rectangular Mindlin plate

δ	$1/\eta$	SCSC	SCSS	SSSS	SCSF	SFSS	SFSF
(m=1,n=1)							
0.01	0.6	67.9041	50.5219	37.2603	18.5719	14.4584	9.5357
	0.8	41.1303	32.0583	25.2794	14.4966	12.6204	9.5861
	1	28.9250	23.6327	19.7322	12.6728	11.6746	9.6270
	1.5	17.3650	15.5730	14.2525	10.9682	10.6654	9.6945
	2	13.6815	12.9152	12.3343	10.4206	10.2948	9.7328
0.1	0.6	56.8967	45.0923	35.0643	17.5196	13.9320	9.3561
	0.8	36.7592	29.8086	24.2330	13.8996	12.2549	9.4047
	1	26.7369	22.4260	19.0840	12.2606	11.3810	9.4458
	1.5	16.6455	15.0884	13.9085	10.7099	10.4404	9.5157
	2	13.2843	12.6022	12.0752	10.2054	10.0929	9.5560
0.2	0.6	41.7529	35.9058	30.4426	15.6184	12.9069	8.9206
	0.8	29.3166	25.3371	21.8089	12.7269	11.4787	8.9621
	1	22.5099	19.7988	17.5055	11.3931	10.7218	8.9997
	1.5	15.0147	13.9113	13.0250	10.1060	9.8971	9.0666
	2	12.3152	11.8061	11.3961	9.6782	9.5902	9.1061
(m=1,n=2)							
0.01	0.6	177.9298	146.8518	119.2771	72.4860	56.0200	23.4448
	0.8	103.6319	86.5136	71.4632	45.5817	36.8242	18.7406
	1	69.1986	58.5687	49.3045	32.9925	27.7042	16.0971
	1.5	35.3123	31.0513	27.4021	20.3073	18.2782	12.9648
	2	23.6327	21.5239	19.7322	15.7393	14.7549	11.6746
0.1	0.6	128.6491	115.0075	100.8535	61.9095	50.7671	21.7604
	0.8	83.7200	73.8005	64.0823	40.9868	34.2963	17.7395
	1	59.4801	52.3247	45.5845	30.4743	26.1910	15.4054
	1.5	32.5876	29.1998	26.1803	19.3498	17.6033	12.5711
	2	22.4260	20.6396	19.0840	15.1956	14.3272	11.3811
0.2	0.6	83.4706	79.8473	75.5553	46.7388	41.9067	19.0838
	0.8	57.2834	55.5966	51.5392	33.3139	29.6359	16.0212
	1	45.0569	41.7813	38.3847	25.8975	23.2429	14.1341
	1.5	27.3400	25.3235	23.4005	17.3888	16.1546	11.7505
	2	19.7988	18.6005	17.5055	13.9934	13.3463	10.7218
(m=2,n=1)							
0.01	0.6	89.6437	76.4781	66.8141	46.8063	44.4696	38.6064
	0.8	65.1670	59.2380	54.8458	43.2079	42.2172	38.7873
	1	54.6743	51.6210	49.3045	41.6472	41.1469	38.9043
	1.5	45.3888	44.5274	43.8305	40.2293	40.0898	39.0679
	2	42.5528	42.2071	41.9144	39.7874	39.7326	39.1526
0.1	0.6	73.8831	66.4133	60.2869	42.7130	41.1136	36.1233
	0.8	57.0503	53.3087	50.3100	39.9417	39.2519	36.3047
	1	49.2606	47.2245	45.5845	38.7128	38.3610	36.4246
	1.5	41.9700	41.3592	40.8467	37.5793	37.4806	36.5941
	2	39.6410	39.3897	39.1713	37.2242	37.1858	36.6824
0.2	0.6	54.3699	51.5078	48.9119	35.7105	34.8930	31.1882
	0.8	44.8507	43.2486	41.8341	33.8972	33.5429	31.3334
	1	40.1384	39.2032	38.3847	33.0747	32.8922	31.4338
	1.5	35.4346	35.1279	34.8558	32.3003	32.2485	31.5782
	2	33.8397	33.7085	33.5896	32.0545	32.0309	31.6538
(m=2,n=2)							
0.01	0.6	201.2858	173.1369	148.7444	103.9515	90.1967	57.7020
	0.8	127.9210	113.4015	100.9808	76.0508	69.1671	50.4009
	1	94.3686	85.9792	78.8455	62.8595	58.9430	46.6393
	1.5	62.2293	59.3935	56.9663	49.6579	48.3432	42.6228
	2	51.6210	50.3833	49.3045	45.0551	44.4758	41.1469
0.1	0.6	128.6491	132.6772	121.7703	85.6022	77.8972	51.6274
	0.8	101.3485	94.0851	87.2358	65.9054	61.6058	45.9146
	1	79.1951	74.4019	70.0219	55.9735	53.3852	42.8870
	1.5	55.6450	53.7714	52.1001	45.5302	44.6033	39.5886
	2	47.2245	46.3599	45.5845	41.7409	41.3217	38.3610
0.2	0.6	93.8549	91.2142	88.3406	63.0974	60.3845	42.1865
	0.8	71.6052	69.2883	66.9264	51.3549	49.5471	38.2999
	1	59.1227	57.3380	55.5860	45.0445	43.8579	36.1646
	1.5	44.7624	43.9183	43.1236	38.0442	37.5757	33.7882
	2	39.2032	38.7801	38.3847	35.3839	35.1634	32.8922